Observation and a model for resonances in one-dimensional unshunted Josephson-junction arrays with ground planes

B. Vasilić,[1] E. Ott,[2] T. Antonsen,[2] P. Barbara,[3] and C. J. Lobb[4]
[1]*Laboratory for Structural NMR Imaging, Department of Radiology, University of Pennsylvania, Philadelphia, Pennsylvania 19104, USA*
[2]*Department of Physics, Department of Electrical and Computer Engineering, and Institute for Research in Electronics and Applied Physics, University of Maryland, College Park, Maryland 20904, USA*
[3]*Georgetown University, Department of Physics, Washington, DC 20057-0995, USA*
[4]*Center for Superconductivity Research, Department of Physics, University of Maryland, College Park, Maryland 20742, USA*
(Received 23 March 2003; published 31 July 2003)

We present data from one-dimensional unshunted Josephson-junction arrays with ground planes, showing resonant behavior for certain values of the critical current. Due to the hysteresis of the current-voltage characteristics, the number of junction that oscillate on resonance can be controlled. The resonant frequency decreases as more junctions are switched onto the resonance and increases as the array length is increased. We develop a transmission-line model of the arrays that reproduces these experimental observations. We also examine the microscopic origin of this model and compare it to existing models in the literature.

DOI: 10.1103/PhysRevB.68.024521 PACS number(s): 74.50.+r, 85.25.Cp, 07.57.Hm, 42.60.Da

I. INTRODUCTION

Since the discovery of the Josephson effect, various resonant phenomena have been observed in Josephson junctions and Josephson-junction arrays. They all reveal themselves through a constant-voltage feature in the current-voltage (I-V) characteristics. This feature is a consequence of the Josephson relations[1]

$$V=\frac{\Phi_0}{2\pi}\frac{d\gamma}{dt}, \quad I=I_C\sin(\gamma), \tag{1}$$

where V and γ are the voltage- and gauge-invariant phase difference across the junction, I the supercurrent flowing through the junction, and I_C and Φ_0 the critical current and magnetic flux quantum.

A constant voltage across a junction is accompanied by supercurrent oscillations with a frequency f that is equal to V/Φ_0. Thus a constant voltage in a Josephson junction or a Josephson-junction array implies the presence of a preferred frequency. (An exception is the gap, a steplike feature in underdamped junctions and arrays which is a consequence of quasiparticle tunneling rather than a resonant effect involving supercurrent oscillations.) There are three ways that a preferred frequency can appear in a system involving Josephson junctions: a resonance internal to the junction can select a frequency, the environment in which the junction is embedded can have resonance frequencies, or an external source can force voltage or current oscillations across the junctions.

Let us consider a junction formed by two parallel slabs of superconductor separated by a thin nonsuperconducting layer. The two superconducting plates form the walls of a transmission line. Depending on the boundary conditions at the edges of the junction and its size, standing or traveling waves can exist inside this transmission line. If standing waves exist, they lead to the well-known Fiske steps,[1] a constant-voltage feature in the I-V characteristic of the junction corresponding to the frequency of the resonant mode. On the other hand, traveling waves in the junction induce the Eck peak.[1] In both of these resonances the junction is interacting with internal modes.

Junctions can also interact with an external resonator, as is the case in the work by Larsen *et al.*[2] The system consisted of a small junction placed inside of a strip-line resonator. The resonant cavity was external to the junction and constant-voltage features were observed in the I-V characteristic at voltages set by the resonant modes of the strip line.

Constant-voltage features can also be observed in junctions which are externally driven. These are the well-known Shapiro steps[1] that occur at integer multiples of the voltage corresponding to the driving frequency. These steps are due to the junction locking to the driving signal and are not resonant in origin.

Underdamped arrays display a variety of geometrical resonances,[3–5] brought about by magnetic fields applied *perpendicular* to the arrays or anisotropies inherent to the arrays. The voltages of these steps are determined by the properties of electromagnetic waves traveling through the discrete structure that the arrays form or the preferred configurations of currents and voltages induced by the applied perpendicular field.

In this work we present experimental observations of a resonance in one-dimensional (1D), underdamped arrays with ground planes above them. We also discuss a transmission-line model that reproduces the main features of the experimental observations. Our resonance is due to the resonant structure formed by the ground plane and junction wiring. The resonance manifests itself through constant-voltage features in the I-V characteristics of the arrays, present only for particular values of the critical current. We have observed[6–8] these self-induced resonant steps (SIRS's) in both 2D and 1D arrays. However, they appear to be different in nature in 1D and 2D arrays and we will only discuss the case of 1D arrays here.

The rest of this paper will be organized as follows: We will first present and discuss data from 1D arrays. We will then introduce a model for the arrays and compare its pre-

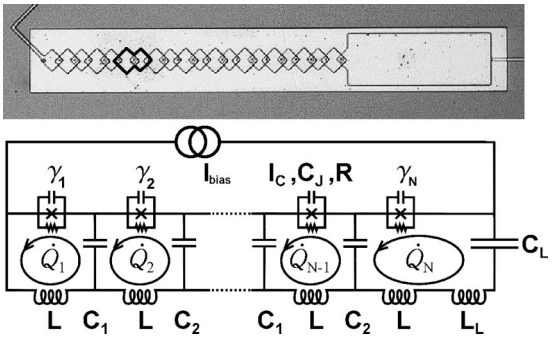

FIG. 1. A micrograph of a one-dimensional array with one unit cell outlined with a thick black line. Below is a circuit schematic of the transmission-line model.

dictions to the data. An approximate model will then be derived and the resulting current-voltage characteristic will be calculated. In Sec. VI the Lagrangian and Hamiltonian of the model will be derived and we will show that they present a full description of the 1D arrays in the relevant limit. A comparison of this model to other works will be made. In the final section we will draw conclusions from an analysis of the data and model.

II. RESONANCES IN ONE-DIMENSIONAL ARRAYS WITH GROUND PLANES

A micrograph of a 1D array with 20 junctions is shown in Fig. 1. The junctions are formed[9] at the overlaps of adjacent niobium squares. At the overlap the squares are separated by an aluminum-oxide tunneling barrier. The right side of the array is terminated by a strip line, while the left side is grounded. The largest, light, rectangle is the niobium ground plane on top of the array. Different niobium layers are separated by silicon dioxide. The dimensions of the squares closer to the ground plane are 12 μm$\times$12 μm, while the ones below them are 16 μm$\times$16 μm. The nominal dimensions of the junctions are 4 μm$\times$4 μm. We current bias the arrays through leads at each end and use the standard four-point technique to measure the voltage.

We observe resonant features only in the *I-V* characteristics of 1D arrays that have specific boundary conditions and a critical current suppressed to about 15 μA by an external magnetic field *parallel* to the junctions. Only arrays with the strip-line termination had the resonance. We analyze these constant-voltage features to determine the dependence of the resonant frequency on the number of junctions *actively* oscillating on resonance and on the *total* number of junctions in the array.

Because of the hysteresis (see Fig. 2) inherent to underdamped junctions, for bias currents below the critical current each junction in the array can have no voltage, the resonant voltage V_{res}, or the gap voltage V_{gap} across it. The junctions that have the resonant voltage across them, and are thus oscillating with the resonant frequency, will be called *active* and their number, will be denoted by N_A. Each time N_A junctions are active a SIRS is present in the *I-V* characteristic at a voltage $N_A V_{res}$, as shown in Fig. 2 for 10- and

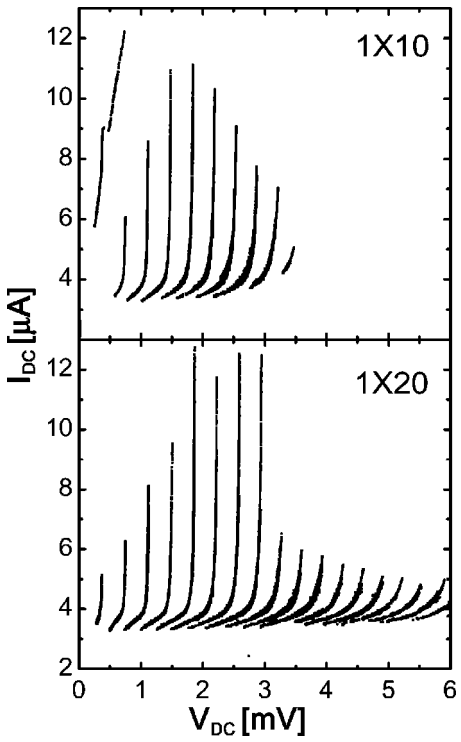

FIG. 2. Current-voltage characteristics of 10-junction (1×10) and 20-junction (1×20) array, when their critical currents are suppressed to about 15 μA. Constant-voltage features are present, corresponding to different numbers of junctions oscillating on resonance. Note that the $V_{gap}\approx2.7$ mV feature is not shown in these graphs.

20-junction arrays and different N_A for each array. For a given array, the step height in current depends on the number of active junctions. For all measured arrays it reaches a maximum for some value of N_A smaller than 20.

A careful inspection of the *I-V* characteristics reveals that the resonant voltage depends on the number of active junctions. To see this more easily, we normalize the voltage of each step by the number of active junctions, N_A, corresponding to it, as shown in Fig. 3 for an array of ten junctions. In this way, we obtain *I-V* characteristics in which the voltage corresponds to the voltage each active junction has when the array is biased on a given SIRS. As the number of active junctions is increased the voltage and frequency of the resonance decrease, as Fig. 3 shows. The same trend is observed for the other measured arrays.

Plots analogous to the one in Fig. 3 are shown in Fig. 4 for an 80-junction array, with each step presented in a separate plot. The steps are shown separately because they split and have a complicated fine structure. We have also observed this fine structure in the smaller arrays; however, in smaller arrays the splitting is much less pronounced. This fact complicates the analysis of the 80-junction array since it is hard to determine which steps correspond to the same resonant feature for different number of active junctions.

In all arrays as we increase the number of active junctions the voltage decreases are very small, less than 5%, which makes the step shape important. We are interested in steps that extend to high currents because they best approach the

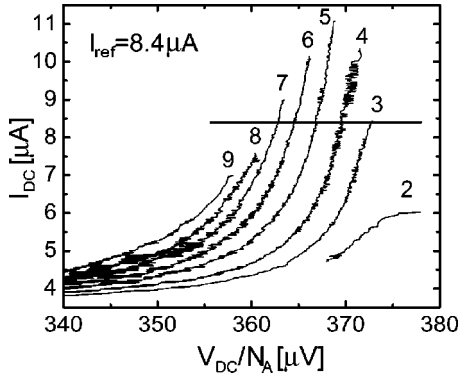

FIG. 3. Current-voltage characteristics for a ten-junction array with the voltage of each constant-voltage feature normalized to the number of junctions oscillating on resonance. The numbers correspond to the number of active junctions for each resonant feature. Note how the resonant voltage decreases as the number of active rows increases. The horizontal line corresponds to the constant-current criterion discussed in the text.

resonant frequency. Since most of the steps are fairly short, we need to optimize the number of steps we want to consider. We record the voltage V_{res} of the selected SIRS at some reference bias current determined by the top of the shortest step in the set of SIRS we have chosen, as in Fig. 3. This criterion is consistent within a single array but is only qualitatively satisfactory when comparing different arrays: in different arrays we choose different optimal currents to reference the step voltages and we do not know how close to the resonant voltage we are at those currents.

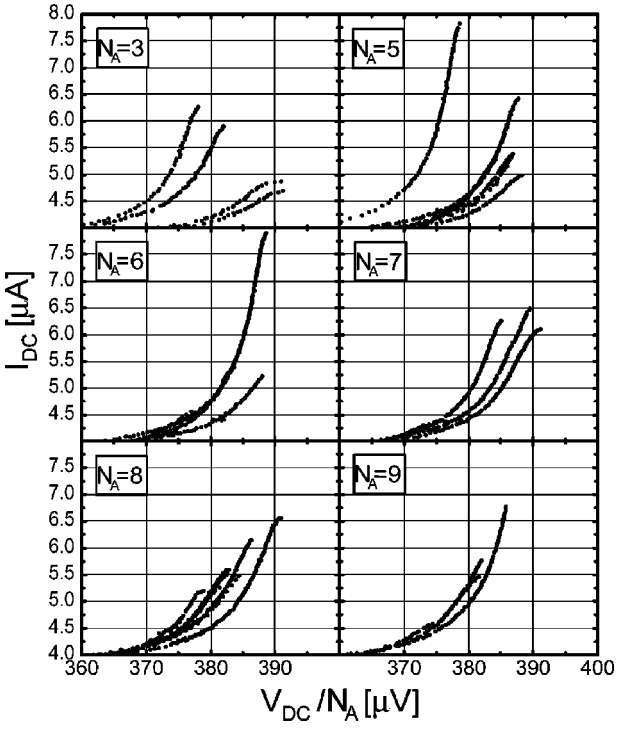

FIG. 4. Detail of the resonant current-voltage characteristics of an 80-junction array. The numbers correspond to the number of active junctions. Note that each constant-voltage feature splits into finer features in this long array.

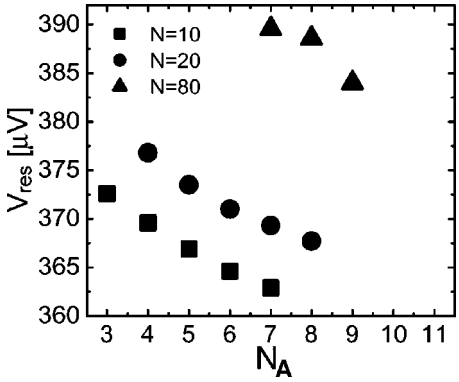

FIG. 5. The resonant voltage of a 10-, 20-, and 80-junction array as a function of the number of active junctions. Note how the resonant voltage increases with the length of the array.

Using data obtained in this way we plot, in Fig. 5, the resonant frequency as a function of the number of active junctions for 10-, 20-, and 80-junction arrays. For the 80-junction array we used only the highest-frequency branches of the seventh, eighth and ninth step, assuming they belong to the same resonant feature. Apart from the previously mentioned decrease of the resonant frequency with the increase of N_A, the second important property of the plot in Fig. 5 is the increase of frequency with array length. While we mentioned in the previous paragraph that we cannot make quantitative comparisons of the frequencies between different arrays, the last conclusion is still qualitatively correct. We checked this by using different reference currents: This always yielded higher frequencies for longer arrays, as did visual inspection of more detailed overlayed plots of the *I-V* characteristics.

III. TRANSMISSION-LINE MODEL

To explain the features of the resonant frequency described in the previous section we use a circuit model[10] of the array that captures the interaction of the junctions and electromagnetic field confined and generated by the ground plane and array. If there is a voltage difference between a niobium square and the ground plane above it, charges will accumulate in the square and ground plane surfaces. There are two different types of squares, in two different niobium layers, that have capacitances C_1 and C_2 with respect to the ground plane as shown in the circuit in Fig. 1. When currents are flowing through the array and through the ground plane, magnetic fields are generated. While the inductance of the two types of squares is different, each junction is surrounded by one square of each kind, so the inductance of each *single* cell in the circuit is the same and equal to L. Because $C_1 \neq C_2$, the *unit* cell of the array consists of two *single-junction* cells.

The left boundary of the circuit is shorted, as is the actual array. The strip line on the right of the array is modeled by a capacitor C_L and an inductor L_L, representing the charges that accumulate on the strip-line plates and the currents along the plates. Each junction is modeled by the RCSJ model.

If there are N junctions in the circuit, the system has $2N$ degrees of freedom, N gauge-invariant phase differences γ_n across the junctions, and N charges Q_n^C on the capacitors. We will introduce effective charges Q_n whose time derivatives are the ac currents flowing through the junctions. These new charges are implicitly defined in terms of the Q_n^C via

$$Q_n^C = Q_n - Q_{n-1}. \tag{2}$$

We introduce Q_n since they yield simpler equations. Using the Josephson relation and equating the voltage drop around each loop to zero, we obtain the following closed system of equations:

$$\frac{\Phi_0 C_J}{2\pi}\ddot{\gamma}_n + \frac{\Phi_0}{2\pi R}\dot{\gamma} + I_C \sin(\gamma_n) = \dot{Q}_n + I_{bias} \quad (n=1,\ldots,N), \tag{3a}$$

$$L\ddot{Q}_n + \frac{\Phi_0}{2\pi}\dot{\gamma}_n + \frac{1}{C_{m(n)}}[Q_n - Q_{n-1}] + \frac{1}{C_{m(n+1)}}[Q_n - Q_{n+1}] = 0, \tag{3b}$$

$$L\ddot{Q}_1 + \frac{\Phi_0}{2\pi}\dot{\gamma}_1 + \frac{1}{C_1}[Q_1 - Q_2] = 0, \tag{3c}$$

$$(L+L_L)\ddot{Q}_N + \frac{\Phi_0}{2\pi}\dot{\gamma}_N + \frac{1}{C_{m(n)}}[Q_N - Q_{N-1}] + \frac{1}{C_L}Q_N = 0, \tag{3d}$$

where an overdot denotes the time derivative d/dt. The index $m(n)$ equals 1 for n even and 2 for n odd. These equations describe a finite portion of a transmission line with Josephson junctions embedded in it. Equation (3c) describes the shorted, left end of the transmission line and Eq. (3d) the right, loaded end.

Normalizing frequencies to $\omega_p = \sqrt{(2\pi I_C)/(\Phi_0 C_J)}$ and currents to the critical current I_C we rewrite Eqs. (3a)–(3d) as

$$\ddot{\gamma}_n + \alpha\dot{\gamma}_n + \sin(\gamma_n) - \dot{q}_n - i_{bias} = 0, \tag{4a}$$

$$\beta_L\ddot{q}_n + \dot{\gamma}_n + \eta_{m(n)}[q_n - q_{n-1}] + \eta_{m(n+1)}[q_n - q_{n+1}] = 0, \tag{4b}$$

$$\beta_L\ddot{q}_1 + \dot{\gamma}_1 + \eta_1[q_1 - q_2] = 0, \tag{4c}$$

$$\beta_L\Lambda\ddot{q}_N + \dot{\gamma}_N + \eta_{m(N)}[q_N - q_{N-1}] + \eta_L q_N = 0, \tag{4d}$$

where an overdot now means a derivative $d/d\tau$ with respect to the dimensionless time τ and with the dimensionless parameters are defined as

$$\beta_L = \frac{2\pi L I_C}{\Phi_0}, \quad \alpha = \sqrt{\frac{\Phi_0}{2\pi I_C R^2 C_J}}, \tag{5}$$

$$\eta_x = \frac{C_J}{C_x} \quad (x=1,2,L), \quad \Lambda = 1 + \frac{L_L}{L}. \tag{6}$$

We will set $\alpha \approx 0$, since the dissipation is small ($\alpha = 0.029$). In order to analyze the resonances of this system we will first linearize the nonlinear Josephson terms. This can be done in two different ways depending on whether a particular junction is active or inactive. For active junctions we will set the nonlinear term equal to zero.[11] Inactive junctions will be modeled by an inductor.[12] For small harmonic oscillations around the equilibrium $[q_n(t) = \tilde{q}_n e^{i\omega t}, \gamma_n(t) = \arcsin(i_{bias}) + \tilde{\gamma}_n e^{i\omega t}]$ and eliminating $\tilde{\gamma}_n$ using the Josephson equations, we obtain the following set of linear equations for the oscillation amplitudes $\tilde{q}_n$:

$$-\omega^2\beta_L\tilde{q}_n + \frac{\omega^2}{\omega^2-\zeta}\tilde{q}_n + \eta_{m(n)}[\tilde{q}_n - \tilde{q}_{n-1}] + \eta_{m(n+1)}[\tilde{q}_n - \tilde{q}_{n+1}] = 0, \tag{7a}$$

$$-\omega^2\beta_L\tilde{q}_1 + \frac{\omega^2}{\omega^2-\zeta}\tilde{q}_1 + \eta_1[\tilde{q}_1 - \tilde{q}_2] = 0, \tag{7b}$$

$$-\omega^2\beta_L\Lambda\tilde{q}_N + \frac{\omega^2}{\omega^2-\zeta}\tilde{q}_N + \eta_{m(N)}[\tilde{q}_N - \tilde{q}_{N-1}] + \eta_L\tilde{q}_N = 0, \tag{7c}$$

where $\zeta \equiv \sqrt{1 - i_{bias}^2}$ and ω is the angular frequency. The corresponding frequency will be denoted with f. These equations are written assuming that all junctions are inactive. If the nth junction is active, ζ will be set equal to zero in the appropriate equation of Eqs. (7a)–(7c), corresponding to an infinite Josephson inductance (the supercurrent channel is open). In the rest of this section the dispersion relations of the infinite linearized system will be derived and an analysis will be presented of the allowed frequencies for the finite system.

We first consider two extreme cases of this linearized system when $N \to \infty$, one in which all of the junctions are active and the other in which all of the junctions are inactive. The infinite linearized transmission line supports traveling waves of the form

$$\tilde{q}_{2m} = \tilde{q}_{even} e^{-i\kappa 2m}, \quad \tilde{q}_{2m+1} = \tilde{q}_{odd} e^{i\kappa(2m+1)}. \tag{8}$$

The dimensionless $\kappa = ka$ is the product of the dimensional wave number k and the length of a single-junction cell, a. We note again that a unit cell of the array consists of two single-junction cells (see Fig. 1).

The dispersion relations obtained by substituting Eq. (8) into Eqs. (7a)–(7c) are given by

$$\kappa(\omega) = \arcsin\left[\frac{1}{2}\left(\frac{1}{\eta_1} + \frac{1}{\eta_2}\right)\left(1 + \frac{1}{\zeta\beta_L - \omega^2}\right)\omega^2 + \frac{1}{4\eta_1\eta_2}\left(1 + \frac{1}{(\zeta\beta_L - \omega^2)} - \frac{2}{\zeta\beta_L - \omega^2}\right)\omega^4\right]. \tag{9}$$

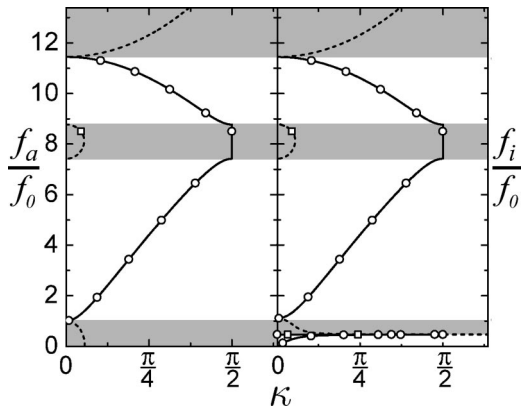

FIG. 6. Dispersion relations for the one-dimensional array when all junctions are active, f_a on the left, and when all junctions are inactive, f_i on the right. Solid lines mark the real part of the wave number κ and dashed lines mark the imaginary part of κ. The open circles and squares mark the real and imaginary parts of κ, respectively, for the allowed frequencies of a ten-junction array. In the shaded regions only evanescent waves exist [$\mathrm{Im}(\kappa)\neq 0$]. Note that κ takes values only up to $\pi/2$.

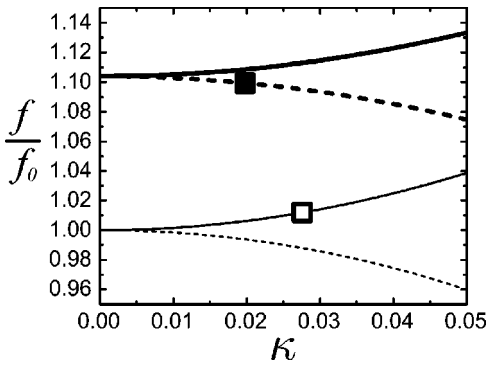

FIG. 7. A detail of the dispersion relations near $\kappa=0$. The solid lines correspond to purely real values of κ (traveling waves) while the dashed lines correspond to purely imaginary values of κ (purely evanescent waves). Two lower-frequency curves correspond to the case when all junctions are active, while the upper two curves correspond to the case when all junctions are inactive. The solid square marks the allowed mode closest to $\kappa=0$ in a ten-junction array for the case when only one junction is active. The open square corresponds to the case when all junctions are active in the same array.

These are shown in Fig. 6, calculated for the fitted values of the parameters given in Table I. How these values were obtained is discussed further in the text. The dispersion relation corresponding to the case of active junctions is denoted by $f_a(\kappa)$, and $f_i(\kappa)$ is the dispersion relation when all junctions are inactive. All frequencies are normalized to

$$f_0=\frac{1}{2\pi}\frac{1}{\sqrt{LC_J}}, \tag{10}$$

which is the frequency corresponding to the $\kappa=0$ mode when all junctions are active. Since the system we are considering is periodic, with a period of two junctions, κ symmetrically takes values in the interval $[-\pi/2,\pi/2]$.

The shaded regions in Fig. 6 mark frequencies for which the excitations are evanescent waves, since κ has a nonzero imaginary part, corresponding to an exponentially decaying or increasing (in space) amplitude of the wave. Frequencies above $8f_0$ are above the gap frequency and would be difficult to excite because of increased dissipation above the gap which lowers the quality factor of the system.

We are interested in frequencies near f_0, since the value of f_0 calculated from our estimates of the array parameters is close to the experimentally observed frequency. Before concentrating on this region of the dispersion relation, one should note two facts. Because of the difference in the capacitances C_1 and C_2, there is a gap in the dispersion (the middle shaded region) in which only evanescent waves exist. When $C_1=C_2$ there is no gap and κ can take values from $[-\pi,\pi]$ because the unit cell of the transmission line is now halved. Also, there is an extra branch in the dispersion for the case of inactive junctions. This branch is present due to the extra degrees of freedom introduced by the Josephson inductances that are present in the inactive junctions.

We will now take a detailed look at the region around f_0, shown in Fig. 7. For a given κ the frequency is always higher for the dispersion corresponding to the case where all junctions are inactive, $f_i(\kappa)>f_a(\kappa)$, as Fig. 7 shows. Therefore, one would expect that as more junctions become active[13] the frequency would grow smaller, similar to the observed behavior shown in Fig. 5, finally reaching the frequency lying on f_a when all junctions are active. To test this idea quantitatively we will next turn to the finite system and calculate the allowed frequencies (normal modes).

Using Mathematica, we calculated the determinant of the system (7a)–(7c) of N linear equations that determine the N oscillation amplitudes $\tilde{q}_n$. The zeros of the determinant are the allowed frequencies of the finite system.[14] We numerically calculated the normal-mode frequencies for different numbers of active junctions and different array lengths in order to make a comparison to the data. (In the experiment, when the array is biased on the N_Ath step we only know that N_A junctions are active but we do not know which particular junctions those are.) For the range of parameters relevant to our systems, the numerically determined frequencies did not change appreciably as we changed the set of N_A active junc-

TABLE I. Nominal values of the array parameters and their values that give the best fit to the data, all calculated for $I_C=30\ \mu$A and $R=150\ \Omega$.

	C_J [fF]	C_1 [fF]	C_2 [fF]	C_L [fF]	L [pH]	L_L [pH]	η_1	η_2	η_L	β_L	Λ	α
Nominal	600±90	10±3	14±3	400±40	2.4±0.5	2.1±0.2	60±24	43±17	1.5±0.4	0.22	1.9±0.5	0.029
Fit	380	10	14	360	2.4	1.9	38	27	1.05	0.22	1.79	0.029

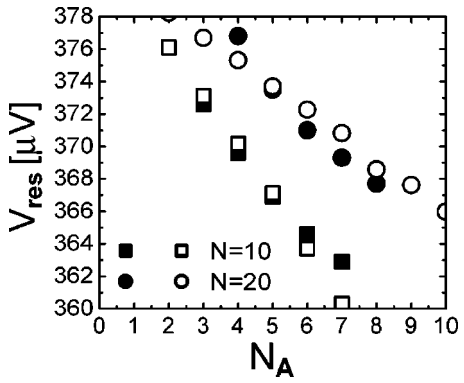

FIG. 8. The resonant voltage as a function of the number of active junctions. Open symbols represent values calculated from the linear limit of the transmission-line model while solid symbols represent measured values for a 10- and 20-junction array.

tions. Because of this, we calculated the frequencies for N_A active junctions using a random choice for their configuration.

The calculated allowed frequencies for the cases when all junctions are active and only one junction is active in a ten-junction array are marked in Figs. 6 and 7. For only one junction active, the frequency of the mode nearest to the $\kappa=0$ mode lies on the part of the dispersion where κ is purely imaginary. This means that the standing wave set up in the space between the array and transmission line is a linear combination of exponentially decaying solutions. For frequencies smaller than, but close to, f_0, the real part of κ is 0 with the decay length larger than the array length, making these evanescent solutions approximately the same as the exact $\kappa=0$ mode. For frequencies larger than, but close to, f_0, shown in Fig. 7, the wavelength of traveling waves is also larger than the array length, making them approximately equivalent to the $\kappa=0$ mode.

Figure 8 shows a comparison between the calculated frequency of the mode closest to $\kappa=0$ and experimental data, for different N_A in two arrays with 10 and 20 total junctions. The fitted parameters that were used in the calculation are given in Table I. They were determined from the array geometry and then adjusted to obtain the best-fit graph in Fig. 8. Nominal and fitted values of the dimensional and their corresponding dimensionless parameters are given in Table I. All but one of the dimensionless fitted parameters are within the error of the nominal estimates. The fitted value of the junction capacitance is not within the error of its nominal estimate. One reason for this is overetching in the fabrication process that diminishes the junction area (and thus the capacitance) and could be seen in micrographs of the arrays.

The calculation correctly predicts the slope of the dependence of the resonant frequency as a function of N_A. It also reproduces the fact that the frequency grows as the array length is increased. This calculation shows that in our arrays the mode nearest to the $\kappa=0$ mode is excited. In the 80-junction array we observed a fine structure in the resonant features, as shown in the first section. The spacing of these fine structure features is similar to the spacing of normal modes near $\kappa=0$, as calculated from the linear transmission-line model. While we do not have a complete understanding of why only modes near $\kappa=0$ are excited, these modes seem physically compelling since at those frequencies all junctions see approximately the same embedding impedance and their phases are all approximately the same.[15]

IV. APPROXIMATE MODEL: ANALYTIC SOLUTIONS

While Eqs. (3a)–(3d) give a complete description of the array, solution is only possible numerically. To make headway, we now derive a reduced set of equations that describes the properties of a state in which N_A of the junctions are active and locked in phase. Two time scales are of importance in the model. First there is a fast time scale given by the high-frequency oscillations at $\omega_0=1/\sqrt{LC_J}$. Each dependent variable in the circuit equations will contain a component oscillating at this frequency. Second, there is a slow time scale that describes the relaxation of the voltages and currents to the locked state. In addition, the slow time scale describes small shifts in frequency of the oscillations from the reference frequency ω_0. According to the assumption of two time scales, we represent the current through the nth junction, $I_n=\dot{Q}_n+I_{bias}$, as follows:

$$I_n(t)=\overline{I_n}(t)+\mathrm{Re}\{\hat{I}_n(t)e^{i\omega_0 t}\}, \tag{11}$$

where we use the convention that a quantity with an overbar is the slowly varying part of a variable and a quantity with a caret is the slowly varying complex amplitude of the oscillatory part of a variable. As a consequence of this representation, each equation in the system (3a)–(3d) will have a high- and a low-frequency version. In order to work with the junction currents I_n instead of the charges Q_n we take the time derivative of Eqs. (3b)–(3d),

$$L\ddot{I}_n+\frac{\Phi_0}{2\pi}\ddot{\gamma}_n+\frac{1}{C_{m(n)}}[I_n-I_{n-1}]+\frac{1}{C_{m(n+1)}}[I_n-I_{n+1}]=0, \tag{12}$$

where the form of this equation for the boundaries is analogous to Eqs. (3c) and (3d).

Like the currents, the gauge-invariant phase of each junction can be expressed in a similar fashion. An important difference between active and inactive junctions is that the phase of active junctions increases steadily with time with rate ω_0. Thus, we write

$$\gamma_n(t)=\omega_0 t+\overline{\gamma_n}(t)+\mathrm{Re}\{\hat{\gamma}_n(t)e^{i\omega_0 t}\} \tag{13a}$$

for active junctions and

$$\gamma_n(t)=\overline{\gamma_n}(t)+\mathrm{Re}\{\hat{\gamma}_n(t)e^{i\omega_0 t}\} \tag{13b}$$

for inactive junctions.

If one substitutes the expressions for junction phase into the formula for the superconducting junction current, one finds that, in general, the junction currents possess a spectrum that includes all harmonics of the reference frequency ω_0. We will retain only the low frequency (average component) of this current and the component at ω_0. Our basis for dropping higher harmonics is the assumption that the array is

being resonantly excited at the frequency ω_0. Thus, its response to this frequency component is large compared with the response to the higher harmonics. Based on this argument we write

$$I_C \sin[\gamma_n(t)] = \overline{I}_{Cn}(t) + \mathrm{Re}\{\hat{I}_{Cn}(t) e^{i\omega_0 t}\}, \tag{14}$$

where for active junctions we have

$$\overline{I}_{Cn} = I_C \frac{J_1(|\hat{\gamma}_n|)}{2|\hat{\gamma}_n|} (\hat{\gamma}_n^* e^{i\overline{\gamma}_n} + \hat{\gamma}_n e^{-i\overline{\gamma}_n}) \tag{15a}$$

and

$$\hat{I}_{Cn} = I_C \frac{e^{i\overline{\gamma}_n}}{i} \left[J_0(|\hat{\gamma}_n|) + J_2(|\hat{\gamma}_n|) \frac{(\hat{\gamma}_n e^{-i\overline{\gamma}_n})^2}{|\hat{\gamma}_n|^2} \right], \tag{15b}$$

while for inactive junctions we have

$$\overline{I}_{Cn} = I_C J_0(|\hat{\gamma}_n|), \tag{15c}$$

$$\hat{I}_{Cn} = I_C \left[\frac{2J_1(|\hat{\gamma}_n|)}{|\hat{\gamma}_n|} \cos\overline{\gamma}_n \right] \hat{\gamma}_n . \tag{15d}$$

In deriving Eqs. (15a)–(15d) we have made use of the Bessel identity

$$e^{iz\cos(\theta)} = \sum_{m=-\infty}^{\infty} J_m(z) e^{im(\theta+\pi/2)}, \tag{16}$$

where $J_m(z)$ is the mth-order, ordinary Bessel function.

We now derive an equation for the oscillating currents in the array. First we consider the high-frequency version of Eq. (12). We substitute expressions (11) and (14) into Eq. (12) and multiply the resulting equation by C_J. After performing the indicated differentiations we only keep terms with up to first time derivatives of $\hat{I}$ and the term that has no time derivatives of the amplitude[16] $\hat{\gamma}$:

$$-\hat{I}_n + \frac{2i}{\omega_0}\frac{d\hat{I}_n}{dt} - \omega^2 \frac{\Phi_0 C_J}{2\pi}\hat{\gamma}_n + \frac{C_J}{C_{m(n)}}[\hat{I}_n - \hat{I}_{n-1}] + \frac{C_J}{C_{m(n+1)}}[\hat{I}_n - \hat{I}_{n+1}] = 0. \tag{17}$$

Again keeping only terms proportional to $\hat{\gamma}$ this amplitude can be expressed by substituting Eqs. (13) and (14) into Eq. (3a):

$$\hat{\gamma}_n = \frac{2\pi}{i\omega_0\Phi_0}\frac{1}{R^{-1} + i\omega_0 C_J}(\hat{I} - \hat{I}_{Cn}). \tag{18}$$

Using Eq. (18) to substitute $\hat{\gamma}_n$ into Eq. (17) we obtain

$$\left(-\frac{1}{1 + i\omega_0 R C_J} + \frac{2i}{\omega_0}\frac{d}{dt} \right)\hat{I}_n + \frac{i\omega_0 R C_J}{1 + i\omega_0 R C_J}\hat{I}_{Cn} + \frac{C_J}{C_{m(n)}}(\hat{I}_n - \hat{I}_{n-1}) + \frac{C_J}{C_{m(n+1)}}(\hat{I}_n - \hat{I}_{n+1}) = 0. \tag{19}$$

For the nominal values of the parameters (Table I) the quality factor describing dissipation in the shunt resistors $Q_R = \omega_0 R C_J \approx 76 \gg 1$, so the previous equation approximates to

$$\frac{2i}{\omega_0}\left(\frac{d}{dt} + \frac{\omega_0}{2Q_R} \right)\hat{I}_n + \frac{C_J}{C_{m(n)}}(\hat{I}_n - \hat{I}_{n-1}) - \frac{C_J}{C_{m(n+1)}}(\hat{I}_{n+1} - \hat{I}_n) = \hat{I}_{Cn}. \tag{20}$$

Equation (20) includes the effects of excitation of the cells by active junctions, the frequency shift induced by inactive junctions, coupling to adjacent cells, and losses due to the junction shunt resistance. Again, we need to modify Eq. (20) to describe the end cells $n=1$ and $n=N$. Since the coupling terms derive from the voltages across the coupling capacitors, these terms are the ones which are modified. In particular, the left side of the array is shorted, implying

$$\frac{2i}{\omega_0}\left(\frac{d}{dt} + \frac{\omega_0}{2Q_R} \right)\hat{I}_1 - \frac{C_J}{C_1}(\hat{I}_2 - \hat{I}_1) = \hat{I}_{C1}. \tag{21a}$$

The right side of the array is connected to a load $Z_L = R_L + iX_L$, which implies

$$\frac{2i}{\omega_0}\left(\frac{d}{dt} + \frac{\omega_0}{2Q_R} \right)\hat{I}_N + \frac{C_J}{C_1}(\hat{I}_N - \hat{I}_{N-1}) + i\omega_0 C_J Z_L \hat{I}_N = \hat{I}_{CN}. \tag{21b}$$

Note that we have now included a resistive part in the load.

Equation (20) along with the boundary conditions (23) determines the structure of the high-frequency mode in the array. In the absence of losses and excitation by the current sources representing the junctions Eq. (20) reproduces the dispersion relation (9) near $\kappa = 0$, shown in Fig. 7. According to our results in Sec. IV, the tendency is for the currents to form a mode in which all the currents are nearly equal. This is a consequence of the coupling being strong, thus forcing the values of current to be close to one another. The values of fluctuating current are not all the same because some junctions are active while other are inactive. Further, power must flow in the direction of the load, which also causes the junction currents to be slightly different. To treat this case in our model we write $\hat{I}_n = \hat{I} + \delta\hat{I}_n$, where $\hat{I}$ is the large common value of current in each cell and $\delta\hat{I}_n$ is the small deviation, which is important only in the coupling terms. We eliminate the unknown deviations by summing Eq. (20) over cell numbers and using the boundary conditions (23). The result is an evolution equation for the common amplitude $\hat{I}$,

$$\frac{2i}{\omega_0}\left(\frac{d}{dt} + \frac{\omega_0}{2Q_R} + \frac{\omega_0^2 C_J Z_L}{2N} \right)\hat{I} = \frac{1}{N}\sum_{n=1}^{N}\hat{I}_{Cn}. \tag{22}$$

Here we see that the load contributes an additional damping mechanism (and frequency shift if it is reactive) that decreases with the number of cells in the array. The term on the right is the sum of the high-frequency components of the junction source current given by Eqs. (15b) or (15d) depending on whether the junction is active or inactive. The effect of the active junctions will be to excite the mode while the

effect of the inactive junctions is to shift its frequency. This will become more apparent when we solve Eq. (22).

We now focus on the low-frequency voltages, currents, and phases. Substituting expressions (14a) and (14b) into the junction equation (4a) and using expansions (15a) and (15c) gives

$$I_{bias}=\overline{I}_n=\frac{\Phi_0 C_J}{2\pi}\frac{d^2\overline{\gamma}_n}{dt^2}+\frac{\Phi_0}{2\pi R}\frac{d\overline{\gamma}_n}{dt}+I_C J_0(|\hat{\gamma}_n|)\sin(\overline{\gamma}_n) \tag{23}$$

for inactive junctions and

$$I_{bias}=\overline{I}_n=\frac{\Phi_0 C_J}{2\pi}\frac{d^2\overline{\gamma}_n}{dt^2}+\frac{\Phi_0}{2\pi R}\left(\frac{d\overline{\gamma}_n}{dt}+\omega_0\right)+I_C\frac{J_1(|\hat{\gamma}_n|)}{2|\hat{\gamma}_n|}(\hat{\gamma}_n^* e^{i\overline{\gamma}_n}+\hat{\gamma}_n e^{-i\overline{\gamma}_n}) \tag{24}$$

for active junctions. These equations, along with mode equation (22) and the relation between oscillating junction phase and array current (18), determine the dynamics of the one-dimensional array of junctions in our reduced model.

V. APPROXIMATE MODEL: EQUILIBRIA

We now look for an equilibrium state in which a specified number of junctions, N_A, is active. It is already clear from our approximate mode evolution equation (22) that only the number of active junctions is important, while their location is irrelevant. We look for solutions in which the phase of the active junctions increases at a slow steady rate,

$$\overline{\gamma}_n(t)=\delta\omega t+\overline{\gamma}_n(0), \tag{25}$$

where $\delta\omega$ represents a small frequency shift from the reference frequency and $\overline{\gamma}_n(0)$ is an initial phase which we will find is the same for all active junctions and whose value is arbitrary. For inactive junctions the frequency shift is absent, and the value of $\overline{\gamma}_n(0)$ will adjust itself according to Eq. (23) to balance the bias current.

We now note that according to Eq. (22) if the quality factor is large, the frequency shift is small compared with the reference frequency, and if the fraction of active junctions is not too small, the fluctuating current excited in each cell will be much larger than the critical current I_C. This is basically a statement that the array is excited resonantly by the active junctions, and it simplifies the calculation of the fluctuating phase given by Eq. (18). Namely, we drop $\hat{I}_{Cn}$ compared with $\hat{I}_n\approx\hat{I}$,

$$\hat{\gamma}_n=-\frac{2\pi}{\omega_0^2\Phi_0 C_J}\hat{I}=-\frac{L}{L_J}\frac{\hat{I}}{I_C}, \tag{26}$$

where we have introduced the nominal inactive junction inductance $L_J=\Phi_0/(2\pi I_C)=L/\beta_L$, where β_L is defined in Eq. (5). We have also used the same approximation as in Eq. (20).

It follows from Eqs. (15b) and (25) that the phase of the oscillating supercurrent for active junctions will advance at the rate $\delta\omega$. In turn, this implies through Eqs. (20) and (26) that the array current and junction phase will also oscillate at this rate. Thus we write

$$\hat{\gamma}_n=\hat{\gamma}_a e^{i[\delta\omega t+\overline{\gamma}_n(0)]}=|\hat{\gamma}_a|e^{i[\phi_\gamma+\delta\omega t+\overline{\gamma}_n(0)]}, \tag{27a}$$

$$\hat{I}=\hat{I}_0 e^{i[\delta\omega t+\overline{\gamma}_n(0)]} \tag{27b}$$

and

$$\hat{I}_{Cn}=-iI_C e^{i[\delta\omega t+\overline{\gamma}_n(0)]}[J_0(|\hat{\gamma}_a|)+J_2(|\hat{\gamma}_a|)e^{2i\phi_\gamma}], \tag{27c}$$

where the complex amplitudes $\hat{\gamma}_a$ and $\hat{I}_0$ are steady in time.

Substituting Eqs. (26) and (32) into expression (22) for the array current yields

$$\frac{\hat{I}_0}{I_C}=-i\frac{N_A Q_T}{N}\frac{J_0(|\hat{\gamma}_a|)+J_2(|\hat{\gamma}_a|)e^{2i\phi_\gamma}}{1+i\Omega}=-\frac{L_J}{L}\hat{\gamma}_a, \tag{28}$$

where

$$\Omega=2Q_T\frac{\delta\omega-\Delta\omega}{\omega_0} \tag{29}$$

represents the frequency shift of the junction oscillations from the array resonance normalized to the total width of the resonance and $Q_T^{-1}=Q_R^{-1}+Q_L^{-1}$ is the total quality factor for the array including local losses due to the shunt resistance (Q_R) and the losses due to the load, $Q_L=N/(\omega_0 C_J R_L)$. Finally, the array resonance is shifted from the reference frequency ω_0 by two effects:

$$\Delta\omega=\frac{\omega_0}{2}\frac{L}{L_J}\frac{N-N_A}{N}\frac{2J(|\hat{\gamma}_a|)}{|\hat{\gamma}_a|}\cos(\overline{\gamma}_n)-\frac{\omega_0 C_J X_L}{2N}. \tag{30}$$

The first term represents the frequency shift due to the inductance of the inactive junctions. This shift is responsible for the dependence of resonant voltage on the number of active junctions shown in Fig. 9. The frequency is upshifted because the inactive junction inductance is effectively added in parallel to the circuit inductance L. The voltages across the coupling capacitors (C_1 and C_2) are all the same for the lowest-order mode of the structure, reducing the total inductance and raising the resonant frequency. The second term represents a frequency shift that depends on the reactive part of the load impedance.

This term is independent of the number of active junctions. The resonant nature of the excitation of the array current is apparent in Eq. (28). The array current will be largest at resonance ($\Omega=0$) and is proportional to the quality factor of the array and the number of active junctions. There is a complicated dependence on the amplitude and phase of $\hat{\gamma}_a$ as contained in the quantity in the square brackets. This will limit the size of the resonance through the relation between the array current and fluctuating junction phase (26). Further,

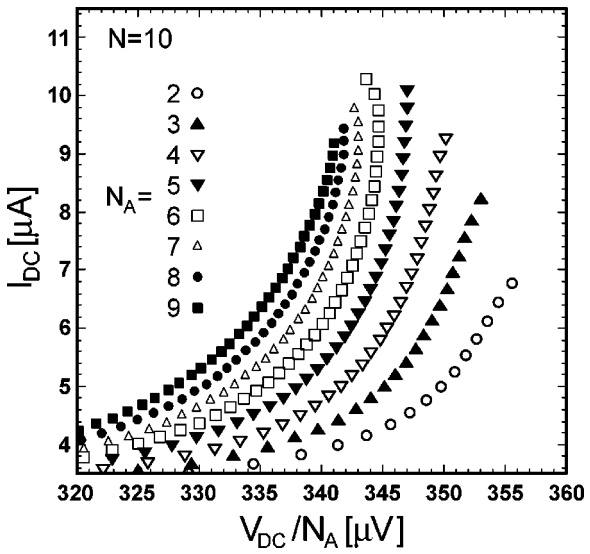

FIG. 9. Normalized current-voltage plots calculated according to Eq. (31). These plots are analogous to the measured ones shown in Fig. 3 and are in good agreement with them. The parameters used to obtain these plots were $I_C=15\ \mu$A, $C_J=380$ fF, $L=2.4$ pH, $R=100\ \Omega$, and $R_L=0.5\ \Omega$.

the location in frequency of the resonance depends on the bias current through Eq. (30). The bias current in equilibrium is determined by Eq. (24) with the slow phase advance inserted:

$$\frac{I_{bias}}{I_C}=\frac{L_J}{R}(\omega_0+\delta\omega)+\frac{J_1(|\hat{\gamma}_a|)}{2|\hat{\gamma}_a|}(\hat{\gamma}_a^*+\hat{\gamma}_a). \tag{31}$$

Numerical solution of the equilibrium equations can be carried out as follows. For a given set of circuit parameters L, L_J, Q_T, and N and for a specified number of active junctions, N_A, Eq. (28) can be solved to find the normalized frequency shift Ω and junction phase ϕ_γ as functions of the quantity $|\hat{\gamma}_a|$. We then compute the array resonance frequency shift $\Delta\omega$ from Eq. (30) assuming the shift due to the reactive part of the load, X_L, is negligible. From Eq. (29) we can find the frequency shift of the locked state, $\delta\omega$. Finally, from Eq. (31) we compute the bias current and plot it versus the per junction voltage $V_{dc}/N_A=(2\pi)^{-1}\Phi_0(\omega_0+\delta\omega)$. Results for representative parameters are displayed in Fig. 9. These can be compared with the experimental results of Fig. 3. As can be seen, the behavior of the measured and calculated current-voltage characteristics is similar. Both plots show a shift to lower voltages with increasing number of junctions. Further, both plots show that the peak current initially increases with the number of active junctions and then saturates. In addition, both plots show that for two active junctions the current-voltage characteristic has a rounded maximum while for a greater number of junctions it develops a cusp.

VI. LAGRANGIAN AND HAMILTONIAN APPROACH: MICROSCOPIC ORIGIN OF THE CIRCUIT MODEL

In this section we introduce the Lagrangian of the system and derive the corresponding Hamiltonian. We also show

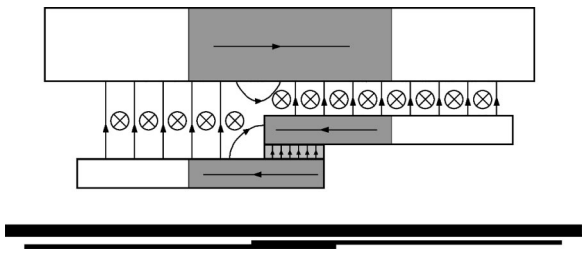

FIG. 10. A schematic of a side view of two niobium squares with the ground plane above them. The lines inside the squares show the currents. The lines in the space between the squares and the ground plane illustrate the electric field lines. The crossed circles represent the magnetic field perpendicular to the plane of the drawing. Below is the same side view drawn to scale.

that the circuit equations (3a)–(3d) completely and accurately describe the 1D arrays in the relevant limit. For notational simplicity we will set $C_1=C_2\equiv C$ which will not influence our conclusions in any significant way.

It is straightforward to check that the Lagrange's equations for the following Lagrangian:

$$\begin{aligned}\mathcal{L}(\gamma_n,\dot{\gamma}_n,Q_n,\dot{Q}_n)&=\frac{C_J}{2}\left(\frac{\Phi_0}{2\pi}\right)^2\sum_{n=1}^{N}\dot{\gamma}_n^2+\frac{L}{2}\sum_{n=1}^{N-1}\dot{Q}_n^2\\&+\frac{L+L_L}{2}\dot{Q}_N^2+I_{bias}\sum_{n=1}^{N}\gamma_n+\frac{\Phi_0 I_C}{2\pi}\sum_{n=1}^{N}\cos(\gamma_n)\\&-\frac{1}{2C}\sum_{n=1}^{N-1}(Q_n-Q_{n+1})^2-\frac{1}{2C_L}Q_N^2-\frac{\Phi_0}{2\pi}\sum_{n=1}^{N}\dot{\gamma}_n Q_n,\end{aligned} \tag{32}$$

reproduce Eqs. (3a)–(3d), excluding dissipative terms. The symbol x_n denotes the whole set of variables $\{x_1,\ldots,x_N\}$.

To analyze the physical origin of the terms in the Lagrangian we will consider all fields and sources in the system. Figure 10 shows a schematic of two squares viewed from the side. The distance from the ground plane to the array ($\approx 0.3\ \mu$m) is much smaller than the lateral dimensions of each square ($>12\ \mu$m). Because of this, the electric field between the array and ground plane only has an appreciable component perpendicular to the ground plane. The magnetic field in this space is also approximately parallel to the ground plane. (The magnetic field also penetrates the superconductors, decaying over a penetration depth λ. This effect is included in the estimate of the inductance of each cell.) These fields are produced by the charges Q_n^C that accumulate on the surfaces of the squares and the currents flowing through them which, due to charge conservation, equal $\dot{Q}_n^C-\dot{Q}_{n+1}^C$. There are also charges that accumulate on the surfaces of the Josephson junctions, producing an electric field perpendicular to the surface of the junction. Since our junctions are small and in the parallel-plate capacitor limit the surface currents are weak and the magnetic field energy

stored in the junction is small, we neglect this higher-order correction to the dominant electric field energy. In the frequency range of interest (close to f_0) each cell is in the lumped limit. This fact and the previously described characteristics of the arrays allow us to model the fields in the arrays as static fields of parallel-plate capacitors and stripline inductors.

We will now show that the Lagrangian (32) accounts for all energies in our system. The first term is the charging energy of the junctions, since the charge across each junction is set by the voltage across the junction which is $(\Phi_0/2\pi)\dot{\gamma}$. The second term is the magnetic energy stored in the space between the ground plane and array. These are the two kinetic terms; the rest are all potential terms. The third term is the Josephson coupling energy present in each junction due to the Josephson effect. The next two terms represent the energy of the electric field present between the array and ground plane. Finally the last term is the interaction term between the two sets of charge distributions: the charges on the junctions and the charges on the square surfaces. This term reflects the fact that these charge distributions are in physical contact so that the charge on one capacitor affects the potential of the other. The fringing fields are small and the energy stored in each capacitor is determined only by its own charge.

To simplify further expressions we set $I_{bias}=0$, $L_L=0$, and $C_L=0$. The assumptions that $C_1=C_2$, $L_L=0$, and $C_L=0$ only affect the spatial dependence (shape) and frequency of the normal modes. These terms can be straightforwardly included in the calculation but do not introduce any changes relevant for the following discussion.

The momentum conjugate to γ_n, $n_n^J=\partial\mathcal{L}/\partial\dot{\gamma}_n$, and the momentum conjugate to Q_n, $\phi_n=\partial\mathcal{L}/\partial\dot{Q}_n$, are

$$\phi_n=L\dot{Q}_n \text{ and } n_n^J=C_J\left(\frac{\Phi_0}{2\pi}\right)^2\dot{\gamma}_n-\frac{\Phi_0}{2\pi}Q_n. \tag{33}$$

After expressing $\dot{\gamma}_n$ as a function of n_n^J and Q_n, and expressing $\dot{Q}_n$ as a function of ϕ_n, one obtains the Hamiltonian corresponding to Eq. (32):

$$\mathcal{H}(\gamma_n,n_n^J;Q_n,\phi_n)=\mathcal{H}_J(\gamma_n,n_n^J)+\mathcal{H}_{TL}(Q_n,\phi_n)+\mathcal{H}_I(n_n^J,Q_n), \tag{34a}$$

$$\mathcal{H}_J(\gamma_n,n_n^J)=\frac{1}{2C_J}\left(\frac{2\pi}{\Phi_0}\right)^2\sum_{n=1}^{N}(n_n^J)^2-\frac{\Phi_0 I_C}{2\pi}\sum_{n=1}^{N}\cos(\gamma_n), \tag{34b}$$

$$\mathcal{H}_{TL}(Q_n,\phi_n)=\frac{1}{2L}\sum_{n=1}^{N}\phi_n^2+\frac{1}{2C}\sum_{n=1}^{N-1}(Q_n-Q_{n+1})^2+\sum_{n=1}^{N}\frac{1}{2C_J}Q_n^2, \tag{34c}$$

$$\mathcal{H}_I(n_n^J,Q_n)=\sum_{n=1}^{N}\frac{2\pi}{\Phi_0}n_n^J\frac{1}{C_J}Q_n. \tag{34d}$$

The potential term of the transmission-line Hamiltonian is a symmetric quadratic form and can be diagonalized. To make this explicit, we introduce a canonical transformation which changes the momenta of the junctions to charges and introduces the normal modes of the transmission line as its coordinates:

$$\gamma_n=\frac{2\pi}{\Phi_0}\Gamma_n,\quad n_n^J=\frac{\Phi_0}{2\pi}q_n^J,\quad Q_n=\sum_{m=1}^{N}M_{nm}q_m,$$
$$\phi_n=\sum_{m=1}^{N}M_{nm}\Phi_m\quad(n=1,\ldots,N). \tag{35}$$

The charge q_n^J conjugate to Γ_n is the charge that gets transferred across the junction only through Cooper-pair tunneling. From its definition and Eq. (33) we see that q_n^J is the difference of charge on the junction capacitor and the charge whose motion generates the total current flowing through the junction. The Hamiltonian in these new coordinates is

$$\mathcal{H}(\Gamma_n,q_n^J,q_n,\Phi_n)=\frac{1}{2C_J}\sum_{n=1}^{N}q_n^{J2}+\frac{1}{2L}\sum_{n=1}^{N}\Phi_n^2-\frac{\Phi_0 I_C}{2\pi}\sum_{n=1}^{N}\cos\left(\frac{2\pi}{\Phi_0}\Gamma_n\right)+\sum_{n=1}^{N}\frac{1}{2C_n^{TL}}q_n^2+\frac{1}{C_J}\sum_{m=1}^{N}q_m\sum_{n=1}^{N}M_{nm}q_n^J, \tag{36}$$

with the capacitances C_n^{TL} defined via the frequencies of the normal modes, $\omega_n=1/\sqrt{LC_n^{TL}}$. The mth column (M_{nm}, $n=1,\ldots,N$) of the matrix M is the mth normal mode of the transmission line. Our system thus consists of the Josephson junctions and the N mutually noninteracting modes of the transmission line. The junctions and normal modes interact through the last term in the Hamiltonian.

When the junctions are in the voltage state in the subgap region, they act as a small harmonic drive to the transmission line. If the frequency of the junction oscillations is not near (within resonance width) any of the normal modes, the transmission line does not get excited. If the junctions oscillate with the frequency of one of the normal modes, that mode gets resonantly excited and a constant-voltage feature is observed in the current-voltage characteristic.

If the modes are well separated, it is sufficient to keep only a single mode in the Hamiltonian, the one near the frequency of interest. Our arrays are finite, discrete systems, with a small number of degrees of freedom and a high quality factor, so the modes are indeed well separated. The Hamiltonian for the case when only the mth mode is excited is

$$\mathcal{H}_m(\Gamma_n,q_n^J,q_m,\Phi_m)=\frac{1}{2C_J}\sum_{n=1}^{N}q_n^{J2}-\frac{\Phi_0 I_C}{2\pi}\sum_{n=1}^{N}\cos\left(\frac{2\pi}{\Phi_0}\Gamma_n\right)+\frac{1}{2L}\Phi_m^2+\frac{1}{2C_m^{TL}}q_m^2+\frac{1}{C_J}q_m\sum_{n=1}^{N}M_{nm}q_n^J. \tag{37}$$

VII. COMPARISON TO OTHER MODELS

The interaction of a Josephson junction or a Josephson-junction array with a single mode of the electromagnetic field has been studied extensively.[17–24] In the past three years researchers have introduced different 1D models[21–24] to describe the operation of our 2D arrays.[6,8] The emphasis in these works was on explaining the high power outputs of the 2D arrays. The model introduced here completely describes the operation of our experimental 1D arrays, and we will compare it to the other models using the derived Lagrangian and Hamiltonian.

The system studied by Filatrella *et al.*[21] is a special case of our transmission-line model. One can check that the Lagrangian and corresponding Hamiltonian (for $I_{bias}=0$) that reproduce the equations used in Ref. 21 are

$$\mathcal{L}_{Fil}(\gamma_n,\dot{\gamma}_n,Q,\dot{Q}) = \frac{C_J}{2}\left(\frac{\Phi_0}{2\pi}\right)^2\sum_{n=1}^{N}\dot{\gamma}_n^2+\frac{L}{2}\dot{Q}^2+\frac{\Phi_0 I_C}{2\pi}\sum_{n=1}^{N}\cos(\gamma_n) - \frac{1}{2C}Q^2-\frac{\Phi_0}{2\pi}\sum_{n=1}^{N}\dot{\gamma}_n Q, \tag{38}$$

$$\mathcal{H}_{Fil}(\Gamma_n,q_n^J;q,\Phi) = \frac{1}{2C_J}\sum_{n=1}^{N}q_n^{J2}+\frac{1}{2L}\Phi^2-\frac{\Phi_0 I_C}{2\pi}\sum_{n=1}^{N}\cos\left(\frac{2\pi}{\Phi_0}\Gamma_n\right) + \frac{1}{2C}q^2+\frac{1}{C_J}q\sum_{n=1}^{N}q_n^J. \tag{39}$$

A comparison of Eq. (39) with Eq. (37) shows that the former is obtained when $M_{nm}=1$, for all n in Eq. (37), which is the case for the $\kappa=0$ mode. Since our system is operating at $\kappa\approx 0$, Eq. (39) is an adequate model for our 1D arrays when they are biased on a constant-voltage feature.

The following Hamiltonian was used by Almaas and Stroud[24]:

$$\mathcal{H}_{Alm}(\phi_m',n_m';q_r',p_r') = \frac{(2e)^2}{C_J}\sum_{m=1}^{N}(n')_m^2+\frac{\hbar\Omega}{2}(p_r')^2-\frac{\Phi_0 I_C}{2\pi}\sum_{m=1}^{N}\cos(\phi_m') + \frac{\hbar\Omega}{2}(g_r')^2+g\hbar\Omega\left(\sum_{m=1}^{N}n_m'\right)^2-\hbar\Omega\sqrt{2g}p_r'\sum_{m=1}^{N}n_m', \tag{40}$$

where one can formally identify[26]

$$n_m'=\frac{q_m^J}{2e},\quad p_r'=\left(\frac{1}{\hbar}\sqrt{\frac{C_m^{TL}}{L}}\right)^{1/2}\Phi, \tag{41a}$$

$$\phi_m'=\frac{2\pi}{\Phi_0}\Gamma_n,\quad q_r'=\left(\frac{1}{\hbar}\sqrt{\frac{L}{C_m^{TL}}}\right)^{1/2}q, \tag{41b}$$

with $\Omega=1/\sqrt{LC_m^{TL}}$ and using the same notation as in Eq. (39). The Hamiltonian (40) looks very similar to the single-mode Hamiltonian of the transmission-line model. However, there are some key differences. The next to last term in Eq. (40), describing the coupling of the mode to the junctions, does not have the same coupling constant as Eq. (37). In the Almaas-Stroud model, the coupling constant g is related to the integral of the vector potential across the junction. This implies that the coupling is mediated through the field that the mode produces *inside* the junction. Also, the last term of Eq. (40) is not present in Eq. (37). This term couples, with equal amplitude, all junction charges. It is not clear to what kind of physical situation this corresponds.

Bonifacio *et al.* considered[19,20] the interaction of a Josephson-junction array with a single mode of the electromagnetic field. The interaction Hamiltonian they used[19] was of the form

$$i\hbar g\left(\hat{a}^\dagger\sum_{n=1}^{N}\hat{S}_n-\hat{a}\sum_{n=1}^{N}\hat{S}_n^\dagger\right), \tag{42}$$

where $\hat{a}^\dagger$ and $\hat{a}$ are the creation and annihilation operators for the resonant mode of the electromagnetic field, with $\hat{S}_n^\dagger$ and $\hat{S}_n$ representing Cooper-pair tunneling from left to right and vice versa across the nth junction. (Unnerstall and Rieckers[25] give an excellent derivation of the Josephson effect and provide much insight into the operator formalism.) To compare to our model we rewrite the interaction term of Eq. (37) in terms of quantum mechanical operators,

$$i\left(\frac{\hbar(2e)^2}{2C_J^2}\sqrt{\frac{C_m^{TL}}{L}}\right)^{1/2}\left(\hat{a}^\dagger\sum_{n=1}^{N}M_{nm}\hat{S}_n^z-\hat{a}\sum_{n=1}^{N}M_{nm}\hat{S}_n^z\right), \tag{43}$$

defining

$$\hat{q}_m\equiv i\left(\frac{\hbar}{2}\sqrt{\frac{C_m^{TL}}{L}}\right)^{1/2}(\hat{a}^\dagger-\hat{a}), \tag{44}$$

$$\hat{\Phi}_m\equiv\left(\frac{\hbar}{2}\sqrt{\frac{L}{C_m^{TL}}}\right)^{1/2}(\hat{a}^\dagger+\hat{a}), \tag{45}$$

$$\frac{\hat{q}_n^J}{2e}\equiv\hat{S}_n^z,\quad \omega_m=\frac{1}{\sqrt{LC_m^{TL}}}, \tag{46}$$

where ω_m is the resonant frequency of the mth normal mode. If we set $M_{mn}=1$ for all n, the difference between Eqs. (42) and (43) becomes apparent. While Eq. (42) has a coupling of the mode to the *supercurrent*, represented by $\hat{S}_n^\dagger$ and $\hat{S}_n$, our Hamiltonian (43) couples the junction *charges* $\hat{S}_n^z$ to the resonant mode.

Interaction terms analogous to Eq. (42), used by various authors,[17,19,20,27] are derived from the expression

$$\int_V \mathbf{j}_s(\mathbf{r})\cdot\mathbf{A}(\mathbf{r})dV, \tag{47}$$

which is the electromagnetic interaction of the Josephson supercurrent $\mathbf{j}_s(\mathbf{r})$ with a normal mode of the field $\mathbf{A}(\mathbf{r})$ inside the junction barrier. This is a distinctly different physical situation then what is present in our arrays, in which the resonant mode is external to the junctions and the energy of the mode is stored in the field between the array and ground plane. Because of this, we find Hamiltonians derived from Eq. (47) inapplicable to our arrays.[28] These Hamiltonians would be appropriate, for example, for an array of junctions that all share a single insulating layer as their tunneling barrier, which is also a dielectric resonator.

VIII. CONCLUSIONS

In measurements of 2D arrays we have observed[6,8] high-efficiency emission of millimeter-wave radiation. A threshold number of active junctions is necessary for coherent radiation to be detected; otherwise, the power is low and incoherent.

The 1D transmission-line model that we have just described does not explain this behavior. The only nonlinear term in Eqs. (3a)–(3d) is the supercurrent in the RCSJ equations, Eq. (3a). As was mentioned before, when the junctions are in the voltage state this term acts as a small harmonic drive to the rest of the equations (3b)–(3d), which are linear. As the oscillation frequency of the active junctions approaches the resonant frequency of the nearest mode the active junctions emit waves that get reflected off the array boundaries and resonantly excite all other junctions. The phases of the junctions are set by the shape of the mode being excited, and as long as the array is biased on a SIRS these phases will remain the same because of the resonant nature of the excitation. We have extensively observed this kind of behavior in numerical simulations of Eqs. (3a)–(3d). In the model, *when the arrays are biased on a constant-voltage feature they are always coherent. There is no threshold in our 1D model.*

We have also developed an analytic model for locked states with a specified number of active junctions. This model successfully reproduces a number of characteristics of the current versus voltage curves observed in the experiment. In particular, the dependence of the shape of the current versus voltage curve on the number of active junctions as well as the peak value of bias current is calculated by the model.

The other models[24,21] described in the previous section show a threshold of a different nature than the one observed in the experiments. In these models the height in current of the resonant features depends on the number of active junctions[29] and decreases with decreasing number of active junctions. If the bias current is too high, for a low number of junctions that have a voltage across them, the resonant state does not exist and the oscillations are not resonant. If the bias current is fixed and the number of active junctions increased, when enough junctions are switched to the voltage state, so that the resonant feature exists, a sudden increase in output power is observed. This is because the junctions switch from the subgap voltage state to the now available resonant state that radiates more power. However, if one is careful to always bias the junctions on a resonant feature, the array is always coherent and *no threshold can be observed as the number of active junctions is varied.*[30]

Even though the synchronization of the 2D arrays remains an open question, the transmission-line model described in this work provides a satisfying description of the 1D arrays. We showed how the linear limit of this model reproduces the observed dependence of the resonant frequency as the number of active junctions, as well as the array length, is varied. The Lagrangian and Hamiltonian for the transmission-line model can be used to compare this model to other models in the literature. The transmission-line model completely describes the physical situation of interest for our arrays, and we believe that its 2D generalization should provide valuable insight into the operation of the radiating 2D arrays.

[1] A. Barone and G. Paternó, *Physics and Applications of the Josephson Effect* (Wiley, New York, 1982).

[2] A. Larsen, H.D. Jensen, and J. Mygind, Physica B **165&166**, 103 (1990).

[3] M. Barahrona, E. Trias, T.P. Orlando, A.E. Duwel, H.S.J. van der Zant, S. Watanabe, and S.H. Strogatz, Phys. Rev. B **55**, R11 989 (1997).

[4] P. Caputo, M.V. Fistul, A.V. Ustinov, B.A. Malomed, and S. Flach, Phys. Rev. B **59**, 14 050 (1999).

[5] A.E. Miroshnichenko, S. Flach, and M.V. Fistul, Phys. Rev. E **64**, 066601 (2001).

[6] P. Barbara, A.B. Cawthorne, S.V. Shitov, and C.J. Lobb, Phys. Rev. Lett. **82**, 1963 (1999).

[7] B. Vasilić, S.V. Shitov, C.J. Lobb, and P. Barbara, Appl. Phys. Lett. **78**, 1137 (2001).

[8] B. Vasilić, P. Barbara, S.V. Shitov, and C.J. Lobb, Phys. Rev. B **65**, 180503 (2002).

[9] All samples were fabricated at HYPRES, Elmsford, NY.

[10] A.B. Cawthorne, P. Barbara, S.V. Shitov, and C.J. Lobb, Phys. Rev. B **60**, 7575 (1999).

[11] B. Vasilić, Ph.D. thesis, University of Maryland, 2002.

[12] K.K. Likharev, *Dynamics of Josephson Junctions and Circuits* (Gordon and Breach, New York, 1986).

[13] This assumes that κ remains approximately the same for different configurations of active and inactive junctions.

[14] Another way to obtain the same result would be to treat the system as consisting of pieces of two different kinds of transmission lines, representing active and inactive junctions. One would then look at transmission and reflection of waves at all the boundaries between different regions and obtain equations for the normal modes. However, this method produces cumbersome transcendental equations which are extremely hard to solve, even numerically, as opposed to the previous method which gives functions in ω whose zeros are easily found by numerical methods.

[15] In an infinite uniform array ($C_1 = C_2 \equiv C$) where all junctions are

active, when $f=f_0$ an interesting effect can be shown to occur. The characteristic impedance of the transmission line goes to zero at $f=f_0$, creating a resonance between L and C_J, and causing all of the ac current generated by an active junction to be coupled into the array. This is clearly advantageous for providing large coupling between junctions.

[16] This is consistent since voltages are proportional to the time derivative of γ leading to an equation with currents and voltages approximated to the same order.

[17] N.R. Werthamer, Phys. Rev. **147**, 255 (1966).

[18] D.R. Tilley, Phys. Lett. **33A**, 205 (1970).

[19] R. Bonifacio, F. Casagrande, and M. Milani, Phys. Lett. **101A**, 427 (1984).

[20] R. Bonifacio, F. Casagrande, and M. Milani, Lett. Nuovo Cimento Soc. Ital. Fis. **34**, 520 (1982).

[21] G. Filatrella, N.F. Pedersen, and K. Wiesenfeld, Phys. Rev. E **61**, 2513 (2000).

[22] J.K. Harbaugh and D. Stroud, Phys. Rev. B **61**, 14 765 (2000).

[23] E. Almaas and D. Stroud, Phys. Rev. B **63**, 144522 (2001).

[24] E. Almaas and D. Stroud, Phys. Rev. B **65**, 134502 (2002).

[25] T. Unnerstall and A. Rieckers, Phys. Rev. B **39**, 2173 (1989).

[26] More on the way Almaas and Stroud derive these equations and the meaning of the different variables can be found in Almaas and Stroud (Ref. 24).

[27] P.A. Lee and M.O. Scully, Phys. Rev. B **3**, 769 (1971).

[28] The work by Tilley treats some very general features which amount to power conservation that should be valid for other Hamiltonians as well.

[29] While in the 1D arrays the height in current of the resonant features depends on the number of active junctions, as described in this work, this is not the case for the radiating 2D arrays. In the 2D arrays all resonant features exist in approximately the same current range.

[30] The authors of Refs. 19 and 21 are in agreement with this interpretation: G. Filatrella, N.F. Pedersen, and D. Stroud (private communication). See also P. Barbara, G. Filatrella, C.J. Lobb, and N.F. Pedersen, in *Studies of High Temperature Superconductors* (NOVA Science, New York, in press).